EXPERIMENTAL HEAT TRANSFER
https://doi.org/10.1080/08916152.2023.2189327

Taylor & Francis
Taylor & Francis Group

OPEN ACCESS Check for updates

Experimental and numerical investigation of direct absorption solar collectors (DASCs) based on carbon black nanofluids

Shihao Wei[a], Lisbeth Espedal[a], Boris V. Balakin[b], and Pawel Kosinski[a]

[a]Department of Physics and Technology, University of Bergen, Bergen, Norway; [b]Department of Mechanical and Marine Engineering, Western Norway University of Applied Sciences, Bergen, Norway

ABSTRACT

Direct absorption solar collectors (DASCs) typically achieve high efficiency due to the volumetric heat absorption process facilitated by the working fluids. In this study, carbon black (CB) nanofluids were utilized as the working fluid to experimentally and numerically investigate the thermal performance of a rectangular DASC. The findings suggest that the nanoparticles have the potential to enhance the efficiency of the DASC.

Direct absorption solar collectors (DASCs) are known for their high efficiency, which is achieved through the volumetric heat absorption process provided by the working fluids In this study, carbon black (CB) nanofluids were used as these working fluids to study the thermal performance of a rectangular DASC. The experiments were conducted using water and nanofluids with 0.05 wt.% nanoparticle concentration, at different flow rates and tilt angles, under a concentrated simulated solar power source. Our results show that the efficiency of the DASC increased as the flow rate increased. The DASC was more efficient when the receiving surface was facing downwards (tilt angle of 0°), and the efficiency was 35% higher than when the receiving surface was facing upwards (tilt angle of 180°). A computational fluid dynamics (CFD) model, which was validated against our experimental results, analyzed the DASC performance under different CB concentrations. According to the simulations, the highest efficiency occurred at a concentration of 0.05 wt.%. The study also highlighted the distribution of temperature and velocity of the nanofluids, as well as the volume fraction of carbon black during the flow process.

ARTICLE HISTORY
Received 27 September 2022
Accepted 3 March 2023

KEYWORDS
Direct absorption solar collector; carbon black; nanofluids; CFD; extinction coefficient

Introduction

With the rapid increase in energy consumption, the need for renewable and clean energy has become urgent [1]]. Solar energy can be considered the best target. Furthermore, equipment that can efficiently capture and utilize solar energy is also in substantial demand [2]. Nowadays, solar energy utilization focuses mainly on converting solar energy into other energy types that can be used directly, such as electricity, heat and fuel [3]. Solar collectors are a type of equipment that can absorb incident solar radiation and convert solar energy into thermal energy [4].

The efficiency of solar collectors relies mainly on the thermal properties of the working fluids inside them. Recently, attempts have been made to exploit nanofluids as working fluids in solar collectors and heat exchange devices [5–7]. Nanofluids are colloidal suspensions of nanometer-sized particles [8] with enhanced thermal properties (relative to the base fluid). Fekadu et al. [9] reported a heat transfer coefficient enhancement of 4.712% and 5.94% for carbon soot nanofluids at a concentration of 0.5% and 0.75%, respectively. They are therefore considered to be promising working fluids [10]. When

CONTACT Pawel Kosinski pawel.kosinski@uib.no Department of Physics and Technology, University of Bergen, Bergen, Norway

© 2023 The Author(s). Published with license by Taylor & Francis Group, LLC.
This is an Open Access article distributed under the terms of the Creative Commons Attribution License (http://creativecommons.org/licenses/by/4.0/), which permits unrestricted use, distribution, and reproduction in any medium, provided the original work is properly cited. The terms on which this article has been published allow the posting of the Accepted Manuscript in a repository by the author(s) or with their consent.

used in direct absorption solar collectors (DASCs), nanofluids offer improved optical absorption of solar heat.

Many researchers have investigated the performance of nanofluids in different solar collectors. Bioucas [11] conducted an experimental study of thermal performance in a flat plate solar collector (FPSC) with different concentrations of nanographene. The maximum efficiency of FPSC was 60.6% when the nanofluid concentration was 0.1 wt.%, compared to 54.7% for the base fluid. This corresponded to a 5.9% enhancement. Sarsam et al. [12] numerically evaluated the properties of multi-wall carbon nanotubes (MWCNT) in an FPSC by the performance index and reported a positive impact on pressure drop. Mwesigye et al. [13] numerically investigated the thermal properties of a parabolic trough solar collector (PTSC) exploiting SWCNT (single-wall carbon nanotubes)-Therminol VP-1-based nanofluids. The results showed a two-fold enhancement of heat transfer performance when using the nanofluid, and the thermal efficiency increased by about 4.4% as the nanoparticle volume fraction rose from 0 to 2.5%. Natividade et al. [14] evaluated the thermal efficiency of an evacuated tube solar collector (ETSC) at low volume fractions of multi-layer graphene (MLG) nanofluids. The thermal efficiency increased by 31% and 76%, corresponding to the concentrations of 0.00045 vol. % and 0.00068 vol. %, compared to the base fluid. Xu et al. [15] explored the performance of a direct absorption solar collector at low temperatures with reduced graphene oxide (RGO)/water-ethylene glycol (EG) nanofluids as working fluids. The nanofluid showed better anti-freeze properties that allowed the DASC to be used in low temperatures, and the efficiency increased by around 70% compared to the base fluid.

Compared to other solar collectors, DASC utilizes fluid as the absorbing medium for incident sunlight, instead of a solid absorber. It can provide greater efficiency than the collectors with surface absorption [16]. Furthermore, various parameters can affect the efficiency of DASC. Bhalla et al. [17] numerically studied the effect of geometrical parameters on the performance of DASC. With an increase in collector length, an apparent efficiency reduction was seen, due to greater heat loss. Sharaf et al. [18] used a suspension of graphite nanoparticles in two different base fluids, including water and Therminol VP-1, to investigate the effect of nanofluid film thickness. Greater efficiency was observed when the depth of the collector was 10 mm, compared to a depth of 0.5 mm. It was also found that the base fluid had an impact on the performance of the collector. When the volume fraction of nanofluids was lower than 0.005%, the water-based nanofluids offered stronger radiation absorption. The base fluid is therefore still an essential factor that affects the thermal efficiency of DASC.

According to the experimental study conducted by Otanicar et al. [19], the solar-weighted absorption efficiencies for water, ethylene glycol (EG), propylene glycol (PG), and Therminol VP-1 were 13.6%, 9.30%, 9.1%, and 2.1%, respectively, measured by a standard scanning wavelength spectrophotometer. Struchalin et al. [20] investigated the thermal performance of carbon-based nanofluids in a tubular DASC experimentally and numerically. The results showed that the efficiency of DASC was at most 37.9% greater than the surface absorption collector. They also discovered that when the flow rate was above 6.0 l/min, the particle deposition was less than 5.0%, from simulation results. The above review indicates that nanofluids can enhance the thermal performance of solar collectors, and most of the research mainly evaluated the impact of the nanofluids' concentration. However, not all the researchers reported positive results for DASCs. Li et al. [21] investigated the thermal performance of a vacuum-packaged volumetric receiver and of a vacuum-packaged black chrome-coated receiver using MWCNT nanofluids at 80°C and 200°C, respectively. The results showed efficiencies of 54% and 26% for the volumetric receiver, which is lower than the surface receiver, with efficiencies of 68% and 47%, respectively. They explained this as optical reflective losses from the outer glass surface. After mathematical calculation, the authors found that only 90% of the effective radiation was transmitted to the glass and absorbed by the nanofluids. Therefore, the anti-reflective coating might be a good option to improve the optical efficiency of the volumetric receiver.

This important discovery was adopted by Struchalin et al. [20] to improve their simulation model that can effectively prevent overpredicting. Nonetheless, it should be noted that the thermal efficiency of solar collectors depends on many factors, such as geometry, base fluid and exposure time. It can

even be affected by the surfactant used to stabilize the nanofluids [22]. Furthermore, nanoparticle material plays a vital role because various nanoparticles have different optical properties. Carbon-based nanomaterials like graphene and nanotubes in particular are excellent anti-corrosion additives for spectrally selective solar absorbers that are an ideal material for the utilization of heat transfer applications [2]. Carbon black (CB) is also a carbon-based nanomaterial with good photothermal properties. In our previous research, we investigated the photothermal properties of CB, such as photothermal conversion [23] and photothermal boiling [24]. Likewise, we experimentally and numerically studied the thermal efficiency of a DASC with Fe_2O_3-based nanofluids [25]. However, to use CB-based nanofluids in a DASC, more knowledge about their optical properties and characteristics needs to be acquired, since little information can be obtained from the literature. Moreover, none of the aforementioned studies were focused on concentrated solar light, so this field needs to be investigated. The light intensity is typically around 1000 W/m^2 on a sunny day, but concentrated solar light intensity can exceed 2000 W/m^2. Therefore, making proper use of concentrated solar light can improve the efficiency of solar energy utilization.

In this work, a series of indoor experiments were conducted to investigate the performance of the DASC based on carbon black (CB) nanofluids under a simulated light source corresponding to concentrated solar light in terms of power. A rectangular DASC with baffles inside the receiver was designed. A halogen lamp was used to simulate the sun and concentrated solar radiation. The temperature histories for different flow rates and tilt angles using both nanofluids and water as base fluids were obtained.

In this study, we developed a volumetric heat transfer model based on Beer-Lambert's law to analyze the flow pattern and distribution of CB nanoparticles in DASCs. The key parameter of our model was the extinction coefficient of CB nanofluids, which we determined by measuring the reduction in heat flux when light passed through the nanofluids. The simulation results showed the behavior and deposition of the nanofluids, and we compared the efficiency of our system with experimental results and some typical commercial models.

Although traditional DASCs used circular cross-section pipes, rectangular channels were commonly used in engineering despite their tendency for uneven heat distribution and nanoparticle deposition. Our study focused on these two issues to improve thermal efficiency, and we combined experimental and simulation methods to investigate the performance of rectangular DASCs. To the best of our knowledge, this aspect has not been adequately addressed in recent research.

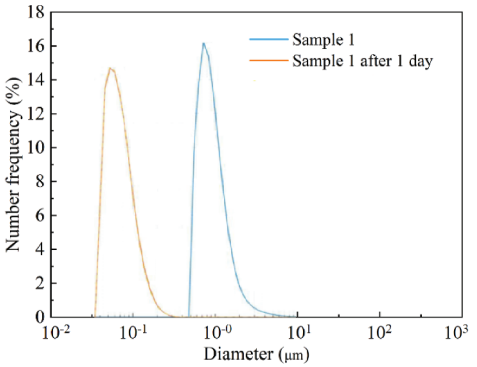
Our findings have important implications for the design and use of commercial DASCs, providing valuable insights into how to optimize their performance."

Experiments

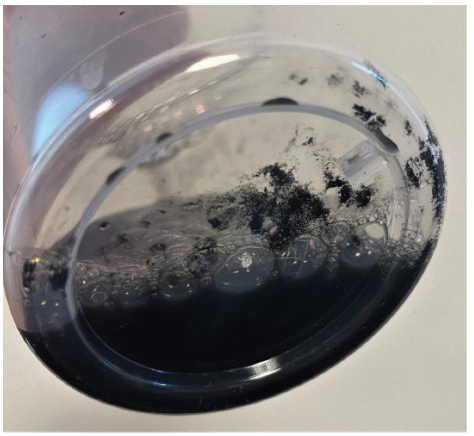
Preparation of nanofluids and stability analysis

A typical two-step method was used to prepare stable CB-based nanofluids. We chose carbon black because its nanofluids are easier to stabilize and have photothermal properties that are less susceptible to environmental factors like temperature, pressure, humidity, and so on. First, CB nanoparticles and SDS were added to distilled water in a beaker. 1.0 wt.% SDS constituted the surfactant that was necessary to stabilize the nanofluids [23]. Secondly, a ceramic magnetic stirrer plate with a maximum stirrer speed of 2000 rpm and a magnetic stirrer bar was used to stir the mixed sample for at least 15 minutes, to acquire a more uniform mixture. Finally, the beaker was put into the tank of an ultrasonic cleaner, so that the liquid in the tank covered the nanofluid. The sample was sonicated for 60 minutes. The cleaner had a frequency of 40 kHz and a maximum power of 335 W, with a maximum capacity equivalent to 6 L. The objective of the process was to break the agglomerates into primary particles. This method has been shown to be effective in numerous scientific papers [21, 23, 24].

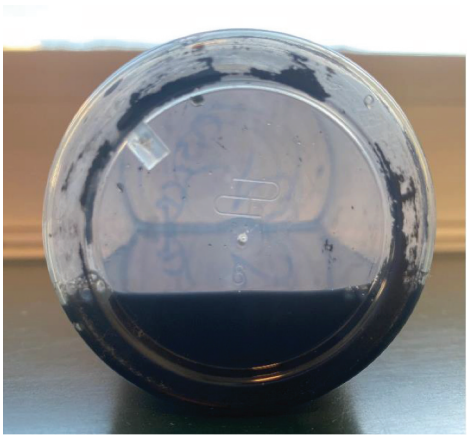
The stability of the prepared nanofluids was evaluated by examining the particle size distribution. To investigate the particle size distribution, we employed the static light scattering (SLS) method, which measures the time-averaged intensity of incident light and determines the particle size distribution over a short period of time. Figure 1(a) shows the particle size distribution for the nanofluid after sonication and after 24 hours, as recorded by Malvern Mastersizer 2000. After the sonication, the particle size distribution was between 480 nm and 10,000 nm, and the average size was around 750 nm. After 24 hours, the particle size range shifted to smaller sizes, apparently due to the deposition of the particles. The particle size range was between 35 nm and 400 nm, and the average size was around 52.4 nm. The maximum particle size number frequency occurred between 50 nm and 60 nm, which corresponds to the CB primary particle size of 51.1 ± 17.0 nm. We also performed a similar measurement of the sample after seven days, but we did not observe any further change in the particle size distribution.



(a) Particle size distribution of the CB nanofluid measured on two consecutive days.



(b) Sedimentation on the container bottom after seven days (a sample was collected after preparation)



(c)Sedimentation on the container bottom after seven days (a sample was collected after the experiments)

Figure 1. Stability analysis of the nanofluids. (a) Particle size distribution of the CB nanofluid measured on two consecutive days. (b) Sedimentation on the container bottom after seven days (a sample was collected after preparation). (c)sedimentation on the container bottom after seven days (a sample was collected after the experiments).

Figure 1 shows sedimentation at the bottom of the container, with (b) depicting sedimentation from a sample after preparation and (c) showing another sample from the reservoir tank after the DASC experimental test. Comparing the two figures, the second sample exhibited a higher level of sedimentation due to damage to the bonding between the surfactant and nanoparticles from repeated heating and circulation during testing, leading to agglomeration and sedimentation. However, the small amount of sediment after seven days indicates the partial long-term stability of the nanofluids. This indicated satisfactory dispersion stability of the CB nanofluids.

Experimental setup

The DASC used in this study comprised three main elements: a glass surface, an inner plate structure with three baffles, and an external aluminum box with hose connectors, as shown in Figure 2. An Osram 400 W/230 V R7S halogen lamp was used to simulate the solar light. The simulated light has non-uniform intensity distribution at the DASC surface. We therefore used the infrared radiometer from Linshang Technology, with an accuracy of±0.10%, to measure the irradiance intensity. Figure 3 shows the intensity distribution on the DASC at a distance of 21 cm from the halogen lamp frame. Using the intensity distribution, we calculated the average intensity to be 1,103 W/m^2, which was slightly higher than the standard solar intensity.

The entire experimental system is depicted in Figure 4. Four Pt100 sensors monitored the inlet and outlet temperatures of the DASC, the ambient temperature and the bulk fluid temperature in the reservoir tank, respectively. The data logger provided a given resolution of 0.001°C and accuracy of 0.015°C. The working fluid was circulated from a 12-l reservoir tank made of thermoplastic material (PMMA) through a 20-m plastic tube. The 12/10-mm tube was made of polytetrafluoroethylene (PTFE), a synthetic fluoropolymer that is a hydrophobic material with a very low friction coefficient. The turbine flow meter was used to control the volumetric flow rate through the system. The flow rate could be adjusted by a flow-control valve placed after the pump. The turbine flow meter used in this work had a given accuracy of 10%. The entire system was insulated thermally to reduce heat loss. The commercial insulation Armaex class 0 SK, with thermal conductivity of K_i = 0.003 W/(m·K), was used in the DASC. The tubes were thermally insulated with 13 mm of polyethylene foam.

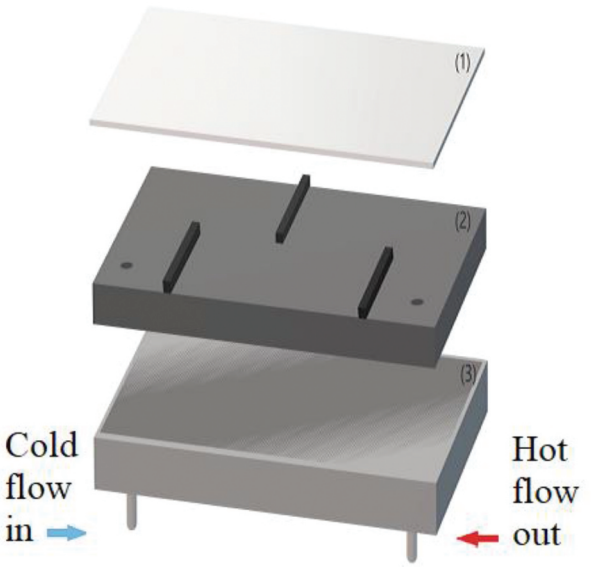


Figure 2. Schematic of the DASC: (1) glass surface, (2) inner plate with three baffles, (3) external aluminum box..

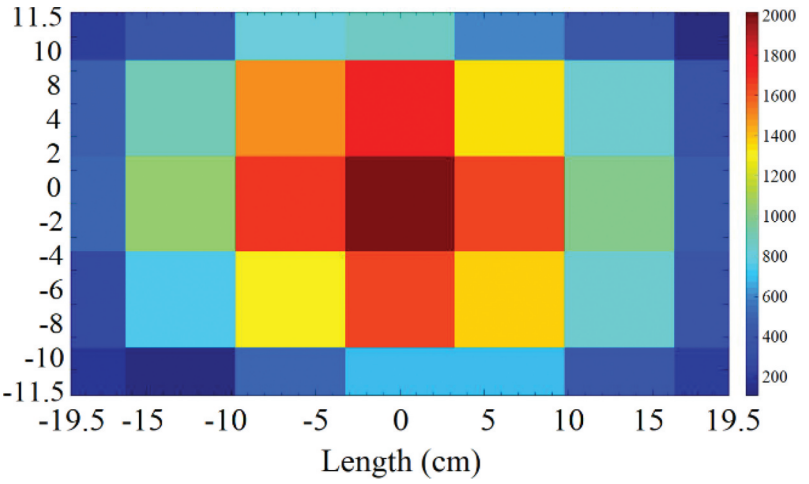


Figure 3. Intensity distribution [W/m^2] on the DASC.

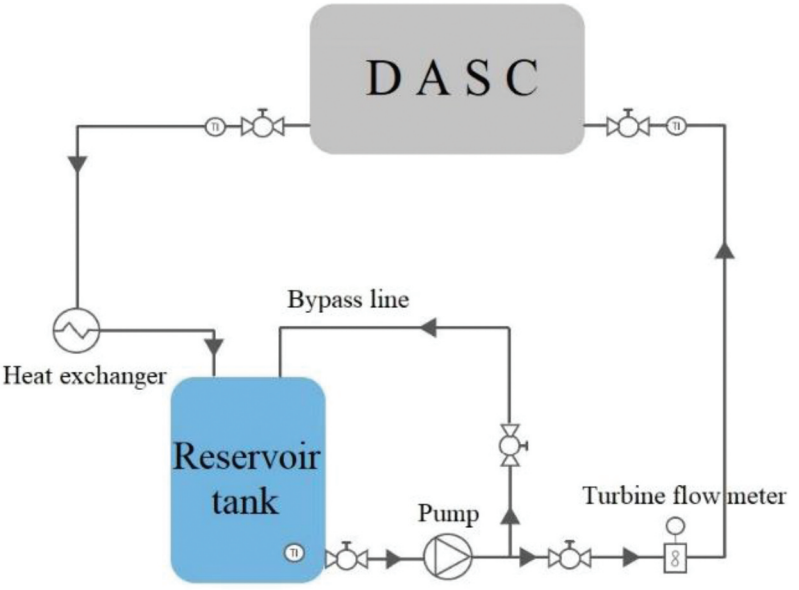


Figure 4. Schematic of the experimental setup.

Experimental procedure

As previously discussed, the fluid (water or nanofluid) was circulated continuously through the system prior to the experiments for two main reasons. This took place primarily to heat the system to a point near thermal equilibrium with its surroundings, and secondarily to avoid the presence of air bubbles in the system. The lamp was turned on immediately after the temperature logging started. During the experiments, all temperatures were sampled every 60 seconds until the DASC inlet and outlet temperatures achieved a steady-state condition. After stabilization, the recording was continued for roughly 100 samples, as this resulted in adequate statistics for each experiment. The four working fluid flow rates chosen for this experimental study were 1 l/min, 2 l/min, 3 l/min and 4 l/min, respectively. For nanofluids, the concentration was 0.05 wt.%. This concentration of CB nanoparticles has been

demonstrated to be optimal in many other scientific papers [21, 24, 26–28]. In addition, a surface absorption experiment was conducted at the flow rates of 0.48 l/min, 1.15 l/min, 1.66 l/min and 2.33 l/min, with water as the working fluid. For this, the glass surface of the collector was covered by black tape. Furthermore, we adjusted the inclination of the DASC by 0°, 15°, 45° and 180°. The inclination angle of 0° referred to the case where the glass surface was oriented along gravity.

The main source of experimental error in this study was the agglomeration of CB nanoparticles. Agglomerates can affect the penetration of light and heat transfer, and even a stable nanofluid cannot completely avoid their formation. During the experiments, the nanofluids were exposed to multiple cycles of heating and circulation, which increased the chance of nanoparticle collision and resulted in agglomeration."

CFD model

Geometry and mesh

For CFD simulations, the computational domain had a rectangular shape with three baffles. The length of the domain was 0.39 m, the width was 0.23 m, and the depth was 0.02 m. The length of the baffles was 0.15 m, and their width was 0.02 m. All the dimensions corresponded to the experimental setup, as shown in Figures 5–6. The fluid entered the domain via a small pipe located in the lower left-hand corner in Figure 5, and the inlet boundary condition was set there. The pressure outlet boundary was located symmetrically on the right-hand side. Both inlet and outlet were connected to the DASC.

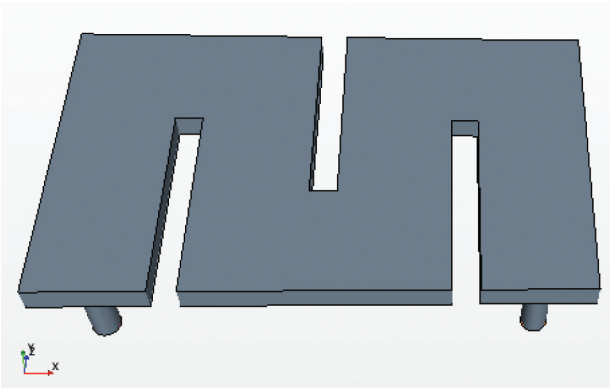


Figure 5. Simulation model of the DASC.



Figure 6. Image of the DASC.

The surface on the opposite side was the receiving surface (glass surface). This surface was irradiated by light and was also subject to heat loss. A trimmed mesh was used when generating the computational cells in the CFD software. The basic size was 0.001 m and the minimum surface size was 0.0001 m, the number of prism layers was 5, and the prism layer total thickness was set as 1/3 with respect to the base size.

Governing equations

We consider an unsteady incompressible flow, described by the Navier-Stokes equations. The continuity equation reads [27]:

$$\frac{D(\alpha_i\rho_i)}{Dt} = 0, \tag{1}$$

where $\frac{D}{Dt}$ is the substantial derivative, α_i is the volume fraction, and ρ_i is density. The subscript i denotes the phases where $i = p$ for the nanoparticle and $i = f$ for the base fluid, $\alpha_f + \alpha_p = 1$.

The momentum equation is given by [28]:

$$\frac{D(\alpha_i\rho_i\boldsymbol{v}_i)}{Dt} = \alpha_i \quad p + \alpha_i\tau_i + \alpha_i\rho_i\boldsymbol{g} + \boldsymbol{F}_{D,ij}, \tag{2}$$

where $\boldsymbol{v}_i$ is the velocity vector, p is the pressure and τ_i is the viscous stress tensor, respectively, $\boldsymbol{g}$ is the acceleration due to gravity and $\boldsymbol{F}_{D,ij}$ is the drag force. Strictly, the motion of nanoparticles should also be affected by Brownian force and thermophoretic force. The Brownian force and thermophoretic force were around at least seven orders and two orders smaller than the drag force, respectively. According to Lutro [29], thermophoretic force has less impact on the nanoparticle motion. Therefore, we assume the Brownian force and thermophoretic force to be negligible. The viscous stress tensor for the particulate phase is computed by the viscosity of the base fluid. This is a viable assumption for low concentrations of carbon-based nanofluids, as confirmed by Struchalin et al. [20].

The drag force was computed as follows [30]:

$$\boldsymbol{F}_{D,ij} = \frac{\pi d^2}{8} N_p\rho_f C_D\left|\boldsymbol{v}_i - \boldsymbol{v}_j\right|\left(\boldsymbol{v}_i - \boldsymbol{v}_j\right), \tag{3}$$

where N_p is the number density for the nanoparticles, d is the diameter of the carbon black nanoparticles and C_D is the drag coefficient computed using the standard expression by Schiller-Naumann [28].

The energy equation is given by [31]:

$$\frac{D(\alpha_i\rho_i(e_i + 0.5|\boldsymbol{v}_i|^2))}{Dt}\mathrm{s} = -\alpha_i \quad \cdot (P\cdot v_i) + \alpha_i \quad \cdot \quad (K_iT_i) + q_{ij} + \alpha_i q_{v,i} + \alpha_i\rho_i\boldsymbol{v}_i\cdot\boldsymbol{g} + \alpha_i \quad \cdot(\tau_i\cdot v_i), \tag{4}$$

where $\boldsymbol{e}_i = C_{p,i}T_i$ is the phase-specific enthalpy, K_i is the thermal conductivity and q_{ij} is the inter-phase heat transfer term. Assuming that the convective heat transfer is established between the phases, the inter-phase heat transfer term is computed according to the Ranz-Marshall expression [28]. Furthermore, q_v is the volumetric heat generation due to the absorption of light. We simplified the thermal re-radiation behavior by assuming that it only occurred at the glass surface of the collector. Likewise, the heat loss only occurred at the glass surface by convection and radiation. Also, we neglected emission and scattering terms for the light in the fluid. The incident heat flux was dissipated as a local heat release. Thus, the volumetric heat generation can be treated as the energy change in the z direction:

$$q_v = -\frac{dI(z)}{dz}, \tag{5}$$

where z is the length of the light path in the z direction, $I(z)$ is the radiative intensity from the glass surface of the incident light, and when z = 0, $I(0)$ represents the intensity of the incident radiation at the glass surface. $I(z)$ can be determined by Beer-Lambert's law [32]:

$$I(z) = I(0)e^{-k_{nf}z}, \tag{6}$$

where k is the extinction coefficient [33], and subscript nf represents the nanofluid. It is the most important parameter of nanofluids.

Following Struchalin et al. [20], the average extinction coefficient of nanofluid at different concentrations can be fit as:

$$k_{nf} = k_f + \alpha_p \mathcal{A}\left(1 + \frac{d^2}{\mathcal{B}}\right), \tag{7}$$

where $\mathcal{A}$ and $\mathcal{B}$ are the fitting constants. Integrating Eq.. (6) and substituting them into Eq.. (5), the volumetric heat generation term reads:

$$q_{v,i} = I(0)k_i e^{-k_{nf}z}, \tag{8}$$

Efficiency

The efficiency of a solar thermal collector is the ratio of collected thermal energy to the total incident energy:

$$\eta = \frac{C_{nf}(T_{out} - T_{in})}{I(0)S}, \tag{9}$$

where η is the efficiency, C_{nf} is the specific heat of nanofluids, is the mass flow rate of the fluid in the collector, T_{out} and T_{in} are the temperatures of the nanofluid at the outlet and inlet, respectively, $I(0)$ is the solar irradiance and S is the solar collector surface area. The specific heat capacity of nanofluids should consider the concentration of the nanoparticles, and it can be calculated by [34]:

$$C_{nf} = \frac{C_p\alpha_p\rho_p + C_f\alpha_f\rho_f}{\alpha_p\rho_p + \alpha_f\rho_f}. \tag{10}$$

Boundary conditions and numerical scheme

The working fluid was a combination of distilled water and CB nanoparticles. Table 1 shows the physical properties of the CB used in this study. These properties, together with the other properties that corresponded to the graphene in the database of the commercial CFD software STAR-CCM, were used to define the nanoparticle in the simulation. IAPWS-IF97 formulation [35] was used to define the thermal properties of the distilled water.

All the surfaces were set as adiabatic, apart from the inlet, the outlet and the glass surface. The environmental temperature and the inlet temperature were set as 300 K and 310.5 K, which

Table 1. Properties of carbon black.

Manufacturer	Bulk density	Specific heat	Average particle size	Thermal conductivity
TIMCAL ENSACO™	2250 kg/m^3	710 J/(kg·K)	60 nm	24 W/(m·K)

correspond to the experimental record. Therefore, the convective heat loss and radiant heat loss at the glass surface can be calculated as in [36]:

$$q_{loss} = h\left(T_{suf} - T_{amb}\right) - \varepsilon\sigma\left({T_{suf}}^4 - {T_{amb}}^4\right), \tag{11}$$

where q_{loss} is the thermal loss, T is the temperature, subscript *suf* and *amb* represent the glass surface and ambient conditions, ε is the emissivity of the receiver (for glass $\varepsilon = 0.85$), σ is the Stefan – Boltzmann constant, and h is the natural convective heat loss coefficient determined by Raleigh number [37]:

$$h = \begin{cases} \left(\frac{K_{nf}}{L}\right)0.54Ra^{\frac{1}{4}}, Ra \le 10^7 \\ \left(\frac{K_{nf}}{L}\right)0.15Ra^{\frac{1}{3}}, Ra > 10^7 \end{cases} \tag{12}$$

In the above, K_{nf} is the thermal conductivity of the nanofluid, L is the length of the DASC, and Ra is the Raleigh number that can be calculated by [38]:

$$Ra = \frac{C_a\left|\frac{\partial \rho_a}{\partial T}\right|\rho_a g\left|T_{suf} - T_{amb}\right|L^3}{K_a\mu_a}, \tag{13}$$

where C_a is the specific heat of air, ρ_a is the density of air, K_a is the thermal conductivity of air, and μ_a is the dynamic viscosity of air.

All the walls were non-slip walls. The ambient temperature was set as 27°C according to the lab environment. The different flow rates of 1 l/min, 2 l/min, 3 l/min and 4 l/min, and the different CB concentrations of 0.01 wt.%, 0.05 wt.%, 0.1 wt.%, 0.5 wt.% and 1 wt.%, were chosen for the numerical study.

Eq. (1) - (5) were solved using STAR-CCM+15.02.007. The numerical solution was obtained using an implicit SIMPLE method. The following relaxation coefficients were applied: 0.3 for pressure, 0.7 for velocity, 0.5 for phase volume fraction, 0.9 for the enthalpy and 0.8 for the turbulence model. The governing equations were discretized temporally with the second-order Euler technique marching at 1.0 ms. The upwind scheme was applied for spatial discretization [28].

Results and discussion

Extinction coefficient

The radiation spectrum of the halogen lamp used in the experiments was measured by Ulset [39]. The maximum intensity of the light from the halogen lamp occurred between the wavelengths of 750–950 nm. In our research, the intensity at different optical path lengths was tested for the CB concentrations of 0.005 wt. %, 0.01 wt. %, 0.05 wt. % and 0.1 wt. %, as shown in Figure 7. The intensity at the optical length of 0 mm represented the intensity of incident light at the nanofluid surface. According to Eq.. (6), the extinction coefficients for different concentrations were calculated, and the results are shown in Figure 8. As follows from the figure, the relationship between the extinction coefficient and the concentration could be roughly approximated by a linear function. This corresponds to Eq.. (7), where the second term in the brackets is in practice negligible, as the particle diameter is very low. A similar result was obtained by Choi et al. [40], who tested the extinction coefficient for different concentrations of carbon nanotube-based nanofluids under the radiation wavelength of 632.8 nm. The results show that when the volume fraction of the carbon nanotube is less than 0.05%, the extinction coefficient increases linearly with the volume fraction, as illustrated by the black line in Figure 8. However, when the volume fraction is greater than 0.05%, the increase is less rapid.

Furthermore, if we compare the red and black curves, we see that the extinction coefficient for carbon nanotubes is less than for carbon black. It must be noted that this result is not only affected by the optical properties of nanoparticles, but also by the wavelengths of light

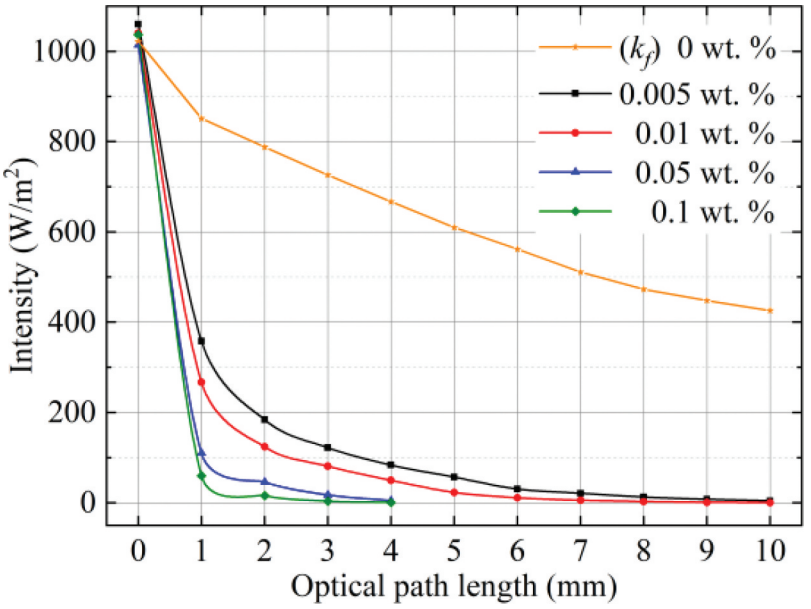


Figure 7. Transmittance of CB nanofluids.

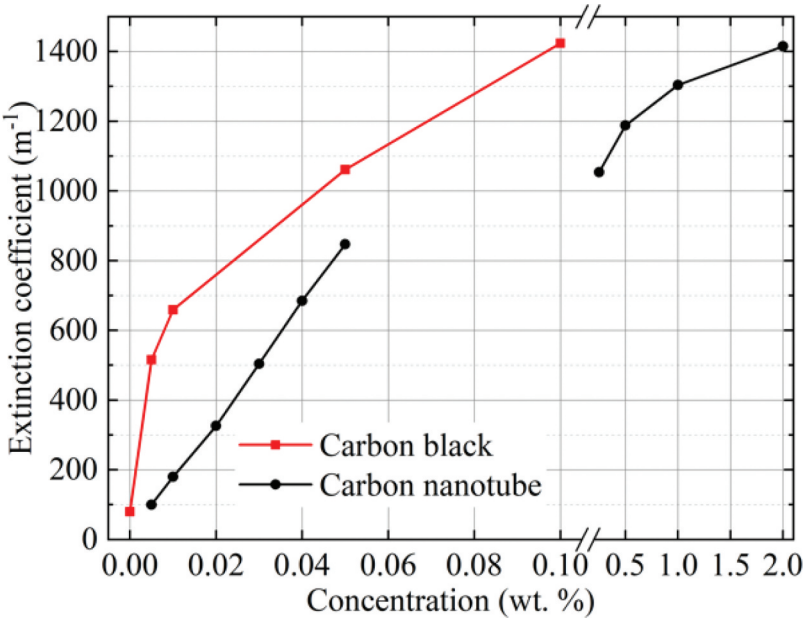


Figure 8. Extinction coefficient of CB nanofluids (red line). The results are compared to the literature results [40] that focused on carbon nanotubes.

sources. This is concluded by Ahmad et al. [41], who investigated the extinction coefficient change on carbon-based nanofluids by varying types of base fluid, and found that when the wavelength increased, the extinction coefficients of all the nanofluids increased. Therefore, the extinction coefficients of the base fluid and nanofluid obtained can be used to complete the volumetric heat transfer model shown in Eq.. (8).

Experimental results

Effect of flow rate

The average temperature change of the working fluids after flowing through the DASC (T_{out} - T_{in}) against time is plotted in Figure 9. When the working fluid is water, the DASC becomes a surface collector, due to the black tape. The solid lines represent the nanofluid, and the dash-dot lines indicate the water. It can be seen that the working fluid temperatures have a clear tendency to rise under the irradiance of concentrated light. With the flow rate increase, the temperature augmentation declines. However, it is easier for nanofluids to reach a stable temperature state. When the system entered into the thermally stable state, we kept recording the temperature for 280 minutes and calculated the average temperature as the final temperature, to evaluate the efficiency. The results are shown in Figure 10. Comparing the average temperature increase, the red line and the green line, the nanofluids show a higher temperature increase at the same flow rate. Hence, the thermal efficiency of the DASC also exceeds the surface collector, and is around 10% at 2 l/min. Following the increase in the flow rate, the total thermal efficiency of nanofluids has an increasing tendency, while for water the opposite applies. In the case of the surface collector, the heat is absorbed by the surface, and transferred by conduction within the water. For the DASC on the other hand, nanoparticles can absorb the irradiance directly, so the heat is transferred by radiation and convection. Therefore, the temperature rises faster and higher for nanofluids. On increasing the flow rate, the residence time for the working fluid inside the collector decreases, and this causes less heat to be absorbed by the working fluid. As a result, the higher the flow rate, the lower the temperature rise. Nevertheless, less residence time also means less heat loss, which leads to higher thermal efficiency for a DASC. However, for the surface collector, the heat is mainly lost from the surface, which has less impact on the residence time of the working fluid. The efficiency of the surface collector therefore decreases with the increase in flow rate. This corresponds to the behavior observed by both Eggers et al. [42] and Gupta et al. [43], who also tested the influence of the flow rate on a DASC. Increasing the flow rate in a DASC system generally leads to greater efficiency, since it reduces the heat loss from the system to the surroundings. However, the dependency is somewhat mitigated, due to the volumetric absorption. For a volumetric absorber, the heat is released within the fluid volume. Eggers et al. [42] explained that most of the incident radiation

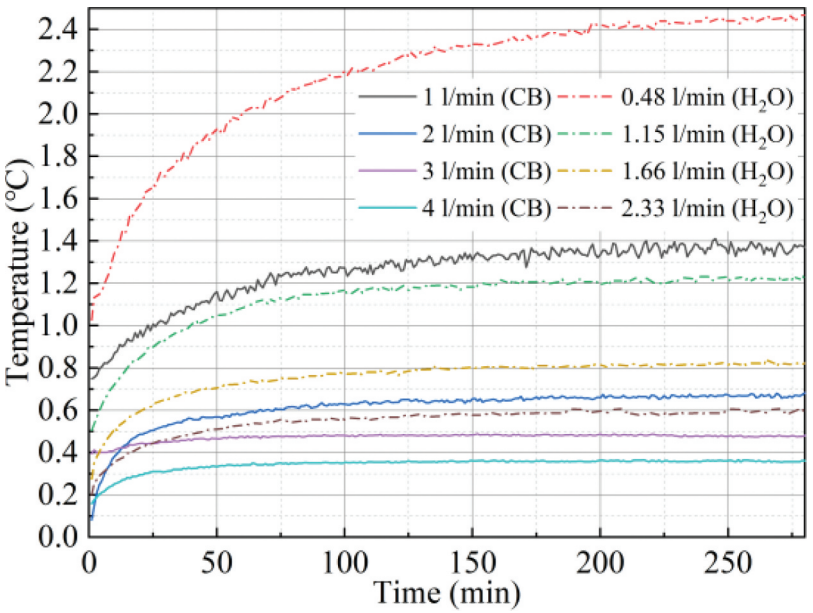


Figure 9. Temperature difference histories in nanofluid and water (C_{CB} = 0.05 wt.%).

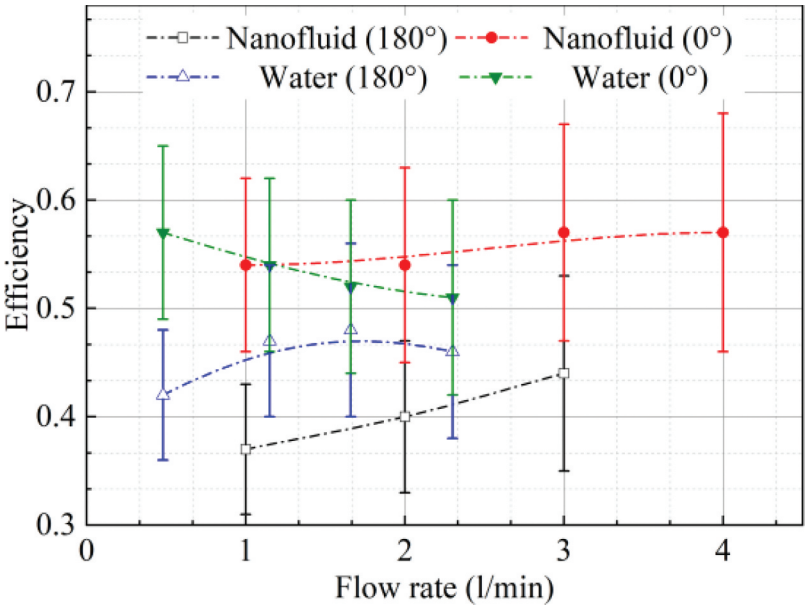


Figure 10. Thermal efficiency at different flow rates and tilt angle for nanofluids and water (C_{CB} = 0.05 wt.%).

absorbed by the fluid volume results in a temperature increase close to the walls, where the average flow rate is lower than at the center of the collector. This results in a temperature rise close to the walls. Our results show agreement with other research that was summarized in the introduction [15, 18, 19].

Effect of tilt angle

In this section, we examine how the inclination of the DASC affects efficiency, and the results are presented in Figure 11. When we incline the DASC, the efficiency change with flow rate tendency

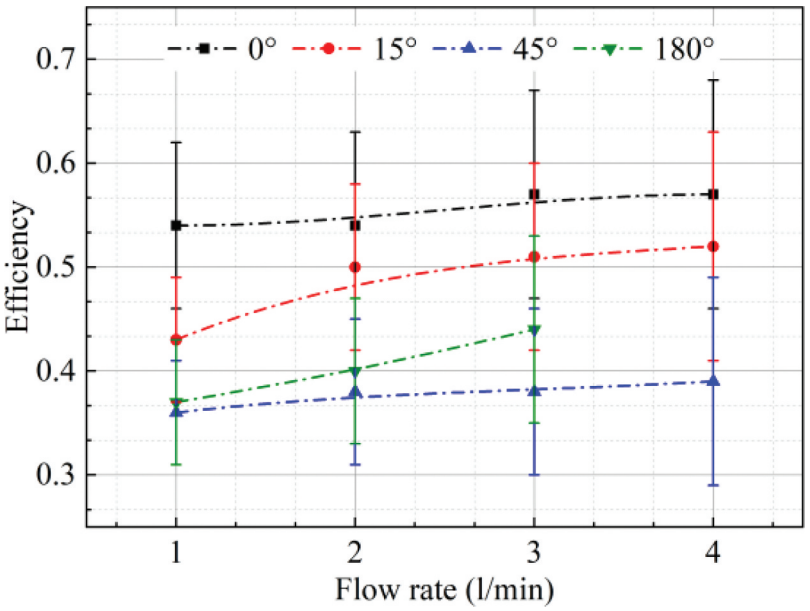


Figure 11. Efficiency of nanofluid at different tilt angles and flow rates (C_{CB} = 0.05 wt.%).

shows agreement with the results of the 0° tilt angle. The maximum efficiency occurs at the tilt angle of 0°, while the efficiency does not decline with the increase in the tilt angle at all ranges. Therefore, the lowest efficiency might exist at a tilt angle. To verify the hypothesis, we predict the change tendency between efficiency and tilt angle in the range of 0°~180°. The black dashed line in Figure 12 is the fitting line, according to our experimental results. With the increase of tilt angle, the efficiency tends to decrease first and then increase, and the minimum efficiency shows between 90° ~ 105°, while the efficiency of the 0° tilt angle is around 35% higher than the 180° tilt angle. This result corresponds to previous research by Balakin et al. [27], as shown in the red line of Figure 12. They numerically investigated the thermal efficiency of a cylindrical column collector with graphene nanofluids (the height is 1.0 cm, and the intensity is 2.3 sun). According to their study, increasing the tilt angle will reduce the convective pattern, until a minimum is reached at 90°, while the collector efficiency increases to a point where the 180° tilt angle is preferred compared to 45°. The comparison between the 0° and 180° tilt angles at different flow rates is also shown in Figure 10.

When the tilt angle is 0°, the DASC is illuminated from the bottom. The outer layer absorbs the heat first, and then a temperature gradient inside the nanofluid is formed. With the increase in temperature, the density of the nanofluid decreases. The buoyant force drives the outer layer nanofluid to move upwards, which leads to macroscopic convection. Wang et al. [44] pointed out that heat transfer is dominated by convection, rather than conduction, in this situation, and this phenomenon is called Rayleigh-Benard convection. Since the direction of the buoyant force is opposite to gravity, the Rayleigh-Benard convection will be affected by inclining the DASC. With the increase in the tilt angle, the angle between buoyance and radiation increases, and the Rayleigh-Benard convection is weakened. Moreover, the working flow can hinder the Rayleigh-Benard convection at the 90° tilt angle. Therefore, the minimum efficiency shows when the tilt angle is 90°. When the tilt angle reaches 180°, the irradiation light comes from the top surface. The heat is absorbed by the top layer and transferred inside the nanofluid by conduction, leading to a higher temperature gradient compared to the 0° tilt angle. Even though the nanoparticles can absorb the heat directly, the Rayleigh-Benard convection is still the predominant factor in reducing the temperature gradient. In this situation, there are numerous heat losses to the environment. Furthermore, Wang et al. [44] also realized that

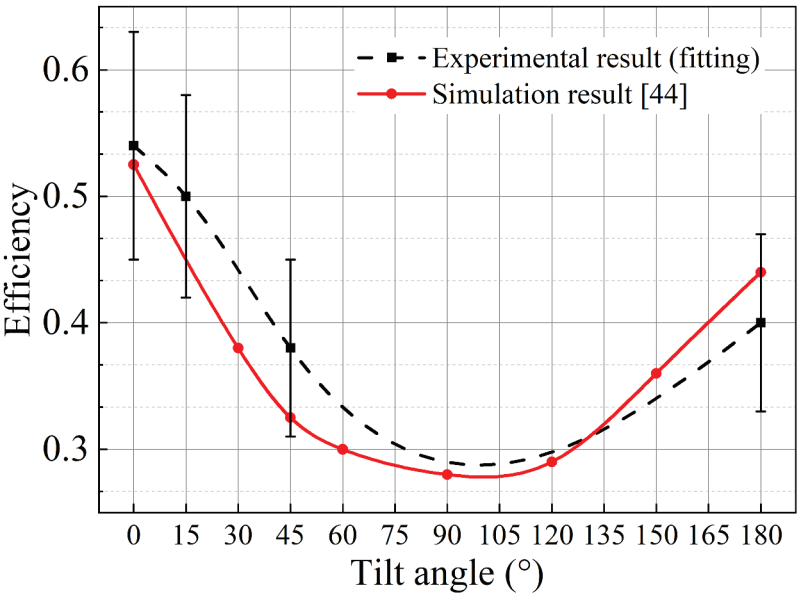


Figure 12. Prediction of the change tendency between efficiency of nanofluid and tilt angles (C_{CB} = 0.05 wt.%, Q = 2 l/min). Compared with Balakin et al. [44].

nanoparticles did not easily form sedimentation when the tilt angle was 0°, because the macroscopic convection made the nanoparticles move continuously. Therefore, the DASC 0° tilt angle has a stronger thermal absorption and conversion ability than the DASC 180° tilt angle.

Model validation

In this research, we also performed CFD simulations using STAR-CCM+, as indicated previously. The efficiencies of the DASC were calculated for all iterations, but the simulation only simulated one iteration. Therefore, we validated the CFD model by comparing the overall temperature increase at the outlet with the experimental results for different flow rates at 0° tilt angle.

We consider laminar flow in the simulations. As shown in Figure 10 for the flow rates of 1 l/min and 2 l/min, the average overall temperature increase is 1.36°C and 0.66°C, respectively.

Table 2 shows the comparison of experimental results and simulation results with flow rates of 1.0 l/min and 2.0 l/min. There is a clear agreement between the simulation results and the experimental results when using CB-based nanofluid as the working fluid. The maximum error was 0.344% when the flow rate was 2.0 l/min. This indicates that the proposed model can be used to analyze the photothermal performance of the DASC for CB-based nanofluids.

Mesh independence study

To ensure mesh independence, we tested five different mesh sizes for our simulation model, following the same strategy as in previous works, including [17, 22, 23]. The mesh sizes studied and grid cell numbers are shown in Table 3. As a critical factor, heat transfer is the most typical parameter we focus on in the simulation. Therefore, we examined the efficiency of the DASC at the glass surface for different mesh sizes [45].

The results are shown in Figure 13. There is a clear tendency for efficiency to decrease due to the increase in cell mesh size. The results showed less precision for larger computational cells, in particular close to the system boundaries, where steep concentration gradients occur. As a result, the interfacial area between nanofluid layers of two different concentrations increased, and more mesh numbers were required to achieve the mesh-independent solutions. Similar results were obtained by Hadjigeorgiou et al. [46], who found that a high concentration gradient existed within each unit cell, except for the last two-unit cells, where the solutions are almost thoroughly mixed. Following the increase in the mesh size, the average Nusselt number rose slightly. The reason was the different boundary conditions for different mesh sizes. The temperature in the cells at the boundary is too high compared to the next cell. This resulted in greater heat loss and also lower thermal efficiency. These results correspond to the paper by Abbassi et al. [47], in which a more refined mesh was needed to achieve mesh-independent results at higher Rayleigh numbers. The average mesh size of 10 mm was therefore chosen to complete the simulation, to ensure mesh independence and reduce the computational cost.

Table 2. Model validation.

Results	1.0 l/min	2.0 l/min
Experiment	1.36°C	0.66°C.
Simulation	1.32°C	0.67°C.
Error	3.03%	−1.49%

Table 3. Mesh numbers for different mesh sizes.

Mesh size (mm)	5	10	15	20	25
Grid cell number	13177488	2690156	944391	463989	285894

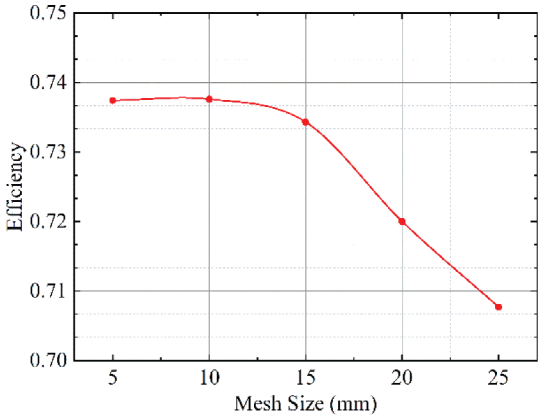


Figure 13. Efficiency vs. mesh size (C_{CB} = 0.05 wt.%, Q = 1 l/min).

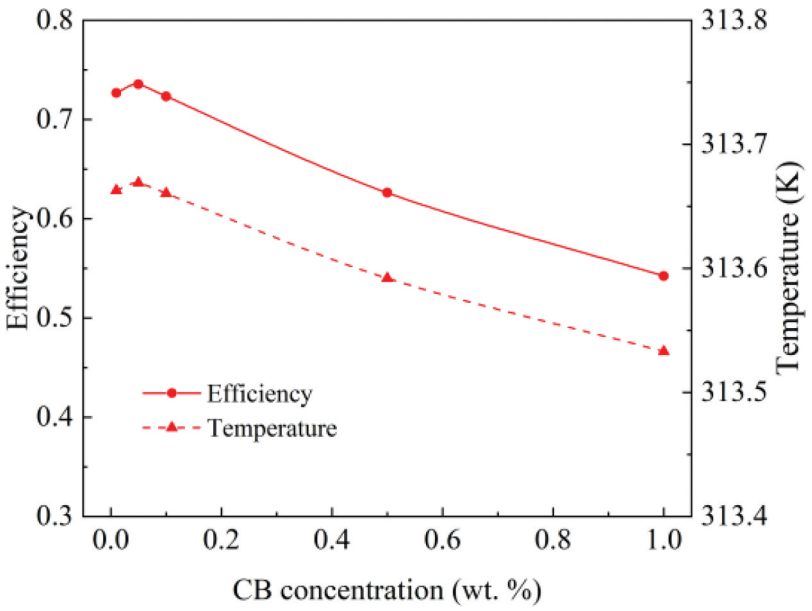


Figure 14. Efficiency for different CB concentrations (Q = 1.0 l/min).fig. 15 .

Simulation results

Effect of CB concentration

Figure 14 shows the thermal efficiency and outlet temperature for different CB concentrations at the flow rate of 1.0 l/min. According to the figure, the efficiency and outlet temperature increase with the CB concentration and reach the maximum of 0.88 and 314.67 K, respectively. This maximum occurs at a CB concentration of 0.05 wt.%. The nanoparticles enhance the absorption of solar radiation in the

base flow. However, as the CB concentration increases further, the efficiency and temperature decrease. When the number of nanoparticles in the base flow is low, the solar light can penetrate the nanofluid and easily reach the upper surface of the DASC. Hence, the fluid layer near the internal surface of the DASC extracts heat from this surface. This results in a more uniform temperature distribution and a lower temperature gradient between the fluid layers. When the concentration is too high, however, there is a large number of nanoparticles that can form a "shield" on the glass surface that blocks the solar light. As a result, only a thin layer of the nanoparticles can absorb the solar radiation directly, and the heat transfer is lower at these concentrations compared to low concentrations within the nanofluid. Accordingly, there will be a larger temperature gradient in these concentrations, causing more heat loss to the surroundings. In our simulation model, all the surfaces were set as adiabatic, except the glass surface, so the heat loss only occurs at the outer layer of this surface. This results in a decrease in the outlet temperature and efficiency. It should be noted that there will have been an optical loss, due to light reflection and glass absorption. Therefore, the actual efficiency and temperature are lower than the simulation results.

Similar results were obtained by some researchers. Otanicar et al. [48] studied the performance of a micro-DASC using an experimental setup and the aqueous suspensions containing silver and graphite nanoparticles and carbon nanotubes as the working fluids. The results show that the collector efficiency is enhanced by the increase in the nanofluid volume fraction because the solar absorption of nanofluid increases. However, this increase continues for a certain amount of volume fraction, and then the reflection of solar radiation from the nanofluid increases, which results in a reduction of efficiency.

Flow patterns

Figs. 15–16(a) show distributions of nanofluid temperature on the middle surface and velocity on the glass surface with a CB concentration of 0.05 wt.% and a flow rate of 2.0 l/min. Due to the viscosity, the velocity on the glass surface and internal surface were almost 0. Therefore, we only show the velocity distribution on the middle surface. The middle surface is located in the middle of the DASC, where the height was 1 mm. At the inlet, the temperature was low and a number of vortices occurred due to the

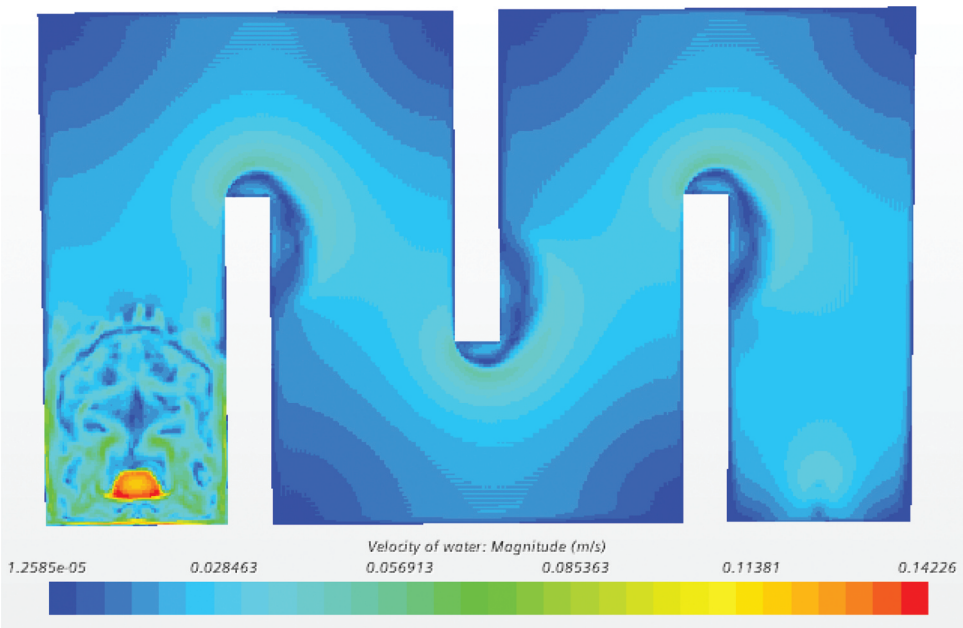


Figure 15. Velocity distribution on the middle surface (height is 1 mm) (C_{CB} = 0.05 wt.%, Q = 2.0 l/min).

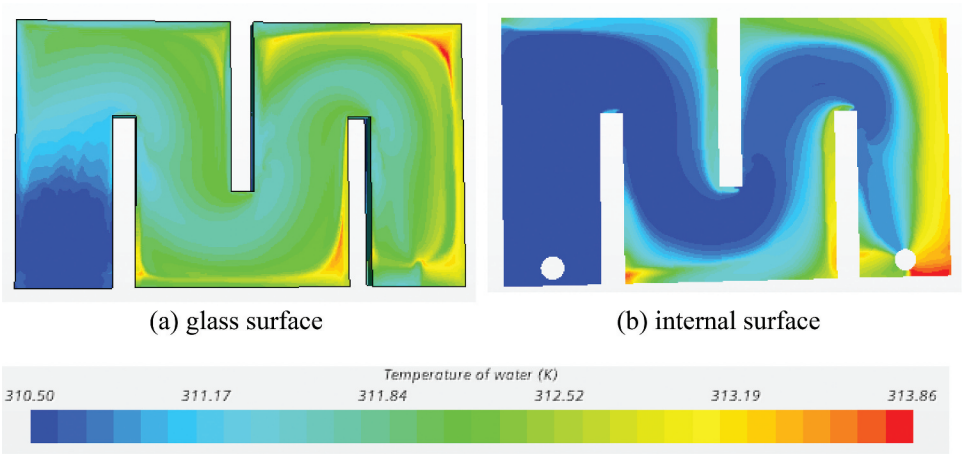


Figure 16. Temperature distribution (C_{CB} = 0.05 wt.%, Q = 2 l/min). (a) glass surface. (b) internal surface.

sudden change in the cross-section radius and flow direction. When the fluid passed the first baffle, the temperature increased, and the velocity direction became clearly defined. The maximum temperature occurred after the third baffle, and the flow showed a clear path to the outlet. By comparing Figures 15 and 16, we see that the area with the higher velocity tended to have a lower temperature. This is due to a shorter thermal exposure time for nanoparticles in these regions.

The presence of the baffles increased the residence time of the nanofluid inside the DASC and thus made it possible to extend the duration of absorption. As can be noted, due to the flow inertia the maximum velocity did not occur in the center of the pipeline. Instead, the maximum velocity was shifted to the right. Therefore, the areas on the opposite side of the baffles had a higher temperature. It is worth emphasizing that in these high-temperature areas, there was a displacement of the fluid toward the internal surface [49]. This phenomenon can be confirmed in Figure 17(a) and Figure 17(b), which show the volume fraction distribution at the glass and internal surfaces. At the glass surface, the volume fraction distribution resembles the velocity field. However, no compaction of particles occurred in the low-velocity regions (compare Figure 15 with 17). As the flow proceeded, it was inevitable that the deposition was formed. In a stable nanofluid, the existence of an electrical double layer (EDL) ensured the repulsion

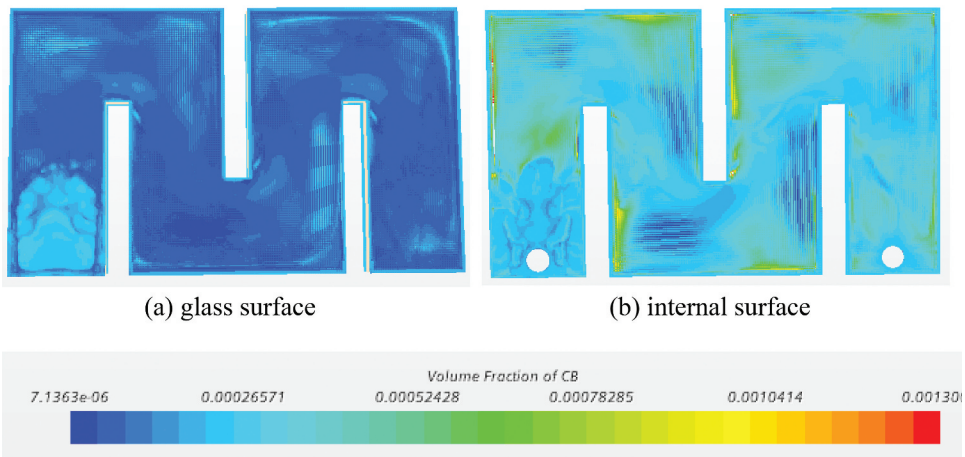


Figure 17. CB volume fraction distribution (C_{CB} = 0.05 wt.%, Q = 2 l/min). (a) glass surface. (b) internal surface.

between nanoparticles. When the stable state was affected by other factors, such as temperature gradient, Brownian motion, buoyancy, etc., that could accelerate the movement of nanoparticles, agglomeration was formed, due to the high chance of collision between nanoparticles. With the growth of the agglomeration, the flow pushed them to deposit near edges and corners. A higher particle volume fraction was thus observed close to the baffles. However, the deposition should occur abundantly on the glass surface due to gravity. In this case, the volume fraction on the internal surface was evidently higher than on the glass surface. Therefore, there must be a heat flow toward the interior of the fluid volume that drives the deposition to move, namely, Rayleigh-Benard convection.

Knowing the distribution of flow patterns could potentially help to increase the efficiency of the DASC for commercial use. The higher temperature makes the DASC more effective, but this is also accompanied by higher heat losses. Therefore, this should be considered when designing DASCs, for example by considering thermal insulation if possible.

Conclusions and future work

In this study, a series of experiments were conducted in a rectangular DASC, to test its thermal performance when using CB-based nanofluids as working fluids at different flow rates and tilt angles. For comparison, a surface collector with water as a working fluid was also used. The thermal efficiency of the DASC showed a rising trend with the flow rate increase and reached 0.57 when the flow rate was 4 l/min. The thermal efficiency of the DASC is higher than the surface collector, and it was 10% higher at 2.0 l/min. Furthermore, the thermal efficiency depends on the DASC orientation in the gravity field with respect to the light source. With the increase of the incline angle of the DASC, the total thermal efficiency decreases, until the tilt angle reaches 90°, and then increases. The results prove that the 0° (down-faced) tilt angle outperforms 180°, and the efficiency is around 35% higher, due to the reduced heat loss and stronger macroscopic convection.

A CFD model of a rectangular DASC was used to analyze the optical properties of CB nanoparticles and the parameters of the DASC. According to the results, CB nanoparticles can increase the absorption of solar radiation in the base flow, and the efficiency of the DASC. As the CB concentration increases, the outlet temperature and efficiency tend to increase first and then decrease. Both the outlet temperature and the efficiency become optimal for the CB concentration of 0.05 wt. %. According to the temperature and velocity distributions, there will be a low flow velocity, but a high-temperature zone, in the rectangular DASC, which can lead to heat loss. Besides, CB nanoparticles will deposit in some places near the internal surface edges, due to the inward heat flow. These reveal the potential improvement for the DASC, to avoid thermal loss.

Optimizing the numerical model is the first objective of our future work. In the future, the efficiencies for different nanofluids and different geometries of DASCs should be considered.

Acknowledgments

Shihao Wei gratefully acknowledges financial support from the China Scholarship Council.

The computations were performed on resources provided by UNINETT Sigma2 - the National Infrastructure for High Performance Computing and Data Storage in Norway.

Boris Balakin thanks the Norwegian Research Council for funding (project 300286).

Disclosure statement

No potential conflict of interest was reported by the author(s).

References

[1] T. B. Johansson, A. P. Patwardhan, N. Nakićenović, and L. Gomez-Echeverri. *Global Energy Assessment: Toward a Sustainable Future*. Cambridge: Cambridge University Press, 2012.

[2] M. Karami, M. Bozorgi, and S. Delfani, "Effect of design and operating parameters on thermal performance of low-temperature direct absorption solar collectors: a review," *J. Therm. Anal Calorim*, vol. 146, no. 3, pp.993–-1013, 2021. DOI: 10.1007/s10973-020-10043-z.

[3] Y. Tripanagnostopoulos, "Photovoltaic/Thermal solar collectors." *Compr. Renewable Energy*, vol. 3, pp. 255–300, 2012.

[4] Z. Haddad, C. Abid, H. F. Oztop, and A. Mataoui, "A review on how the researchers prepare their nanofluids," *Int. J. Thermal Sci*, vol. 76, pp. 168–189, 2014. DOI: 10.1016/j.ijthermalsci.2013.08.010.

[5] G. Peker, C. Yıldız, G. Çakmak, Y. Bilgiç, and A. Yıldız. "Thermal performance of new type plate heat exchanger with spring turbulence generator using nanofluid flow." *Exp. Heat Transfer*. 1–15. May, 2022. 10.1080/08916152.2022.2081886

[6] R. A. Abu Talib and S. Salman, "Heat transfer and fluid flow analysis over the microscale backward-facing step using β Ga 2 O 3 nanoparticles." *Exp. Heat Transfer*, vol. 36, no. 3, pp. 1–18, Feb. 2022. DOI: 10.1080/08916152.2022.2039328.

[7] S. M. Hm and R. N. Hegde, "Investigations on the effect of disturbed flow using differently configured turbulators and Alumina nanofluid as a coolant in a double tube heat exchanger." *Exp. Heat Transfer*, vol. 35, no. 3, pp. 282–307, Apr. 2022. DOI: 10.1080/08916152.2020.1860159.

[8] R. Saidur, K. Leong, and H. A. Mohammed, "A review on applications and challenges of nanofluids," *Renewable Sustainable Energy Rev.*, vol. 15, no. 3, pp.1646–1668, 2011. DOI: 10.1016/j.rser.2010.11.035.

[9] B. Fekadu, R. Kathiravan, and P. Saravanan, "Augmentation of pool boiling heat transfer characteristics using naphtha carbon soot nanoparticles–water based nanofluids," *Exp. Heat Transfer*, vol. 35, no. 6, pp.1–16, 2021. DOI: 10.1080/08916152.2021.1958108.

[10] R. Maithani, R. Agarwal, A. Kumar, and S. SharmaParametric optimization of impinging air jet on hemispherical protrusion of a solar thermal collector*Exp. Heat Transfer*1–22May202210.1080/08916152.2022.2075989

[11] F. Bioucas, S. Vieira, M. Lourenço, F. Santos, and C. N. de Castro, "Performance of heat transfer fluids with nanographene in a pilot solar collector," *Solar Energy*, vol. 172, pp. 171–176, 2018. DOI: 10.1016/j.solener.2018.05.040.

[12] W. S. Sarsam, S. Kazi, and A. Badarudin, "Thermal performance of a flat-plate solar collector using aqueous colloidal dispersions of multi-walled carbon nanotubes with different outside diameters," *Exp. Heat Transfer*, vol. 35, no. 3, pp.258–281, 2022. DOI: 10.1080/08916152.2020.1847215.

[13] A. Mwesigye, İ. H. Yılmaz, and J. P. Meyer, "Numerical analysis of the thermal and thermodynamic performance of a parabolic trough solar collector using SWCNTs-Therminol® VP-1 nanofluid," *Renewable Energy*, vol. 119, pp. 844–862, 2018. DOI: 10.1016/j.renene.2017.10.047.

[14] P. S. G. Natividade, *et al.*, "Experimental analysis applied to an evacuated tube solar collector equipped with parabolic concentrator using multilayer graphene-based nanofluids," *Renewable Energy*, vol. 138, pp. 152–160, 2019. DOI: 10.1016/j.renene.2019.01.091.

[15] X. Xu, C. Xu, J. Liu, X. Fang, and Z. Zhang, "A direct absorption solar collector based on a water-ethylene glycol based nanofluid with anti-freeze property and excellent dispersion stability," *Renewable Energy*, vol. 133, pp. 760–769, 2019. DOI: 10.1016/j.renene.2018.10.073.

[16] C. H. Li and G. Peterson, "Experimental investigation of temperature and volume fraction variations on the effective thermal conductivity of nanoparticle suspensions (nanofluids)," *J. Appl. Phys.*, vol. 99, no. 8, pp.084314, 2006. DOI: 10.1063/1.2191571.

[17] V. Bhalla, V. Khullar, and H. Tyagi, "Investigation of factors influencing the performance of nanofluid-based direct absorption solar collector using Taguchi method," *J. Therm Anal Calorim*, vol. 135, no. 2, pp.1493–1505, 2019. DOI: 10.1007/s10973-018-7721-x.

[18] O. Z. Sharaf, D. C. Kyritsis, A. N. Al-Khateeb, and E. Abu-Nada, "Effect of bottom surface optical boundary conditions on nanofluid-based DASC: parametric study and optimization," *Solar Energy*, vol. 164, pp. 210–223, 2018. DOI: 10.1016/j.solener.2018.02.052.

[19] T. P. Otanicar, P. E. Phelan, and J. S. Golden, "Optical properties of liquids for direct absorption solar thermal energy systems," *Solar Energy*, vol. 83, no. 7, pp.969–977, 2009. DOI: 10.1016/j.solener.2008.12.009.

[20] X. Li, *et al.* "Numerical analysis of photothermal conversion performance of MXene nanofluid in direct absorption solar collectors." *Energy Convers. Manage.*, vol. 226, pp. 113515, 2020. DOI: 10.1016/j.enconman.2020.113515.

[21] P. Struchalin, *et al.* "Performance of a tubular direct absorption solar collector with a carbon-based nanofluid." *Int. J. Heat Mass Transf*, vol. 179, pp. 121717, 2021. DOI: 10.1016/j.ijheatmasstransfer.2021.121717.

[22] T. J. Choi, S. P. Jang, and M. Kedzierski, "Effect of surfactants on the stability and solar thermal absorption characteristics of water-based nanofluids with multi-walled carbon nanotubes," *Int. J. Heat Mass Transf*, vol. 122, pp. 483–490, 2018. DOI: 10.1016/j.ijheatmasstransfer.2018.01.141.

[23] A. Kosinska, B. V. Balakin, and P. Kosinski, "Photothermal conversion of biodegradable fluids and carbon black nanofluids," *Sci. Rep*, vol. 12, no. 1, pp.1–13, 2022. DOI: 10.1038/s41598-022-07469-w.
[24] E. T. Ulset, *et al*., "Photothermal boiling in aqueous nanofluids," *Nano Energy*, vol. 50, pp. 339–346, 2018. DOI: 10.1016/j.nanoen.2018.05.050.
[25] A. Sözen, M. Gürü, T. Menlik, U. Karakaya, and E. Çiftçi, "Experimental comparison of Triton X-100 and sodium dodecyl benzene sulfonate surfactants on thermal performance of TiO2–deionized water nanofluid in a thermosiphon," *Exp. Heat Transfer*, vol. 31, no. 5, pp.450–469, 2018. DOI: 10.1080/08916152.2018.1445673.
[26] B. V. Balakin, M. Stava, and A. Kosinska, "Photothermal convection of a magnetic nanofluid in a direct absorption solar collector," *Solar Energy*, vol. 239, pp. 33–39, 2022. DOI: 10.1016/j.solener.2022.04.027.
[27] B. V. Balakin, O. V. Zhdaneev, A. Kosinska, and K. V. Kutsenko, "Direct absorption solar collector with magnetic nanofluid: cFD model and parametric analysis," *Renewable Energy*, vol. 136, pp. 23–32, 2019. DOI: 10.1016/j.renene.2018.12.095.
[28] R. Bårdsgård, D. M. Kuzmenkov, P. Kosinski, and B. Balakin, "Eulerian CFD model of direct absorption solar collector with nanofluid," *J. Renewable Sustainable Energy*, vol. 12, no. 3, pp.033701, 2020. DOI: 10.1063/1.5144737.
[29] H. F. Lutro. "The effect of thermophoresis on the particle deposition on a cylinder," 2012.
[30] T. Cosgrove. *Colloid Science: Principles, Methods and Applications*. Hoboken, New Jersey, United States: John Wiley & Sons, 2010.
[31] H. M. Al-Ali and N. H. HamzaNumerical and experimental study of the influence of extended surfaces in rectangular channel subjected to constant heat flux*Exp. Heat Transfer*1–19Feb202310.1080/08916152.2023.2176567
[32] M. Kalteh, A. Abbassi, M. Saffar-Avval, and J. Harting, "Eulerian–eulerian two-phase numerical simulation of nanofluid laminar forced convection in a microchannel," International journal of heat and fluid flow, vol. 32, no. 1, pp. 107–116, 2011.
[33] C. F. Bohren and D. R. Huffman. *Absorption and Scattering of Light by Small Particles*. New York: John Wiley & Sons, 2008.
[34] R. A. Taylor, P. E. Phelan, T. P. Otanicar, R. Adrian, and R. Prasher, "Nanofluid optical property characterization: towards efficient direct absorption solar collectors," *Nanoscale Res. Lett*, vol. 6, no. 1, pp.1–11, 2011. DOI: 10.1186/1556-276X-6-225.
[35] IAPWS, TGD8-16, *Application of Film Forming Substances in Fossil, Combined Cycle, and Biomass Power Plants*. Colorado, United States: The International Association for the Properties of Water and Steam, 2019.
[36] A. Lenert and E. N. Wang, "Optimization of nanofluid volumetric receivers for solar thermal energy conversion," *Solar Energy*, vol. 86, no. 1, pp.253–265, 2012. DOI: 10.1016/j.solener.2011.09.029.
[37] T. L. Bergman, T. L. Bergman, F. P. Incropera, D. P. Dewitt, and A. S. Lavine. *Fundamentals of Heat and Mass Transfer*. New York, United States: John Wiley & Sons, 2011.
[38] J. Liu, Z. Ye, L. Zhang, X. Fang, and Z. Zhang, "A combined numerical and experimental study on graphene/ionic liquid nanofluid based direct absorption solar collector," *Solar Energy Mater. Solar Cells*, vol. 136, pp. 177–186, 2015. DOI: 10.1016/j.solmat.2015.01.013.
[39] E. T. Ulset. "Utilizing solar vapour energy by use of nanofluids in a direct absorption solar collector," University of Bergen, Bergen, Norway, 2018.
[40] T. J. Choi, S. H. Kim, S. P. Jang, L. Lin, and M. A. Kedzierski, "Aqueous nanofluids containing paraffin-filled MWCNTs for improving effective specific heat and extinction coefficient," *Energy*, vol. 210, pp. 118523, 2020. DOI: 10.1016/j.energy.2020.118523.
[41] S. Ahmad, R. Saidur, I. Mahbubul, and F. Al-Sulaiman, "Optical properties of various nanofluids used in solar collector: a review," *Renewable Sustainable Energy Rev.*, vol. 73, pp. 1014–1030, 2017. DOI: 10.1016/j.rser.2017.01.173.
[42] J. R. Eggers, E. M. Lange, and S. Kabelac, "Radiation and energetic analysis of nanofluid based volumetric absorbers for concentrated solar power," *Nanomaterials*, vol. 8, no. 10, pp.838, 2018. DOI: 10.3390/nano8100838.
[43] H. K. Gupta, G. D. Agrawal, and J. Mathur, "An experimental investigation of a low temperature Al2O3-H2O nanofluid based direct absorption solar collector," *Solar Energy*, vol. 118, pp. 390–396, 2015. DOI: 10.1016/j.solener.2015.04.041.
[44] K. Wang, *et al*. "Significant photothermal conversion enhancement of nanofluids induced by Rayleigh-Bénard convection for direct absorption solar collectors." *Appl. Energy*, vol. 254, pp. 113706, 2019. DOI: 10.1016/j.apenergy.2019.113706.
[45] M. Hatami and D. Jing, "Evaluation of wavy direct absorption solar collector (DASC) performance using different nanofluids," *J. Mol. Liq*, vol. 229, pp. 203–211, 2017. DOI: 10.1016/j.molliq.2016.12.072.
[46] A. G. Hadjigeorgiou, A. G. Boudouvis, and G. Kokkoris, "Thorough computational analysis of the staggered herringbone micromixer reveals transport mechanisms and enables mixing efficiency-based improved design," *Chem. Eng. J.*, vol. 414, pp. 128775, 2021. DOI: 10.1016/j.cej.2021.128775.
[47] M. A. Abbassi, *et al*., "LBM simulation of free convection in a nanofluid filled incinerator containing a hot block," *Int. J. Mech. Sci.*, vol. 144, pp. 172–185, 2018. DOI: 10.1016/j.ijmecsci.2018.05.031.

[48] T. P. Otanicar, P. E. Phelan, R. S. Prasher, G. Rosengarten, and R. A. Taylor, "Nanofluid-based direct absorption solar collector," *J. Renewable Sustainable Energy*, vol. 2, no. 3, pp.033102, 2010. DOI: 10.1063/1.3429737.

[49] M. Simonetti, F. Restagno, E. Sani, and M. Noussan, "Numerical investigation of direct absorption solar collectors (DASC), based on carbon-nanohorn nanofluids, for low temperature applications," *Solar Energy*, vol. 195, pp. 166–175, 2020. DOI: 10.1016/j.solener.2019.11.044.